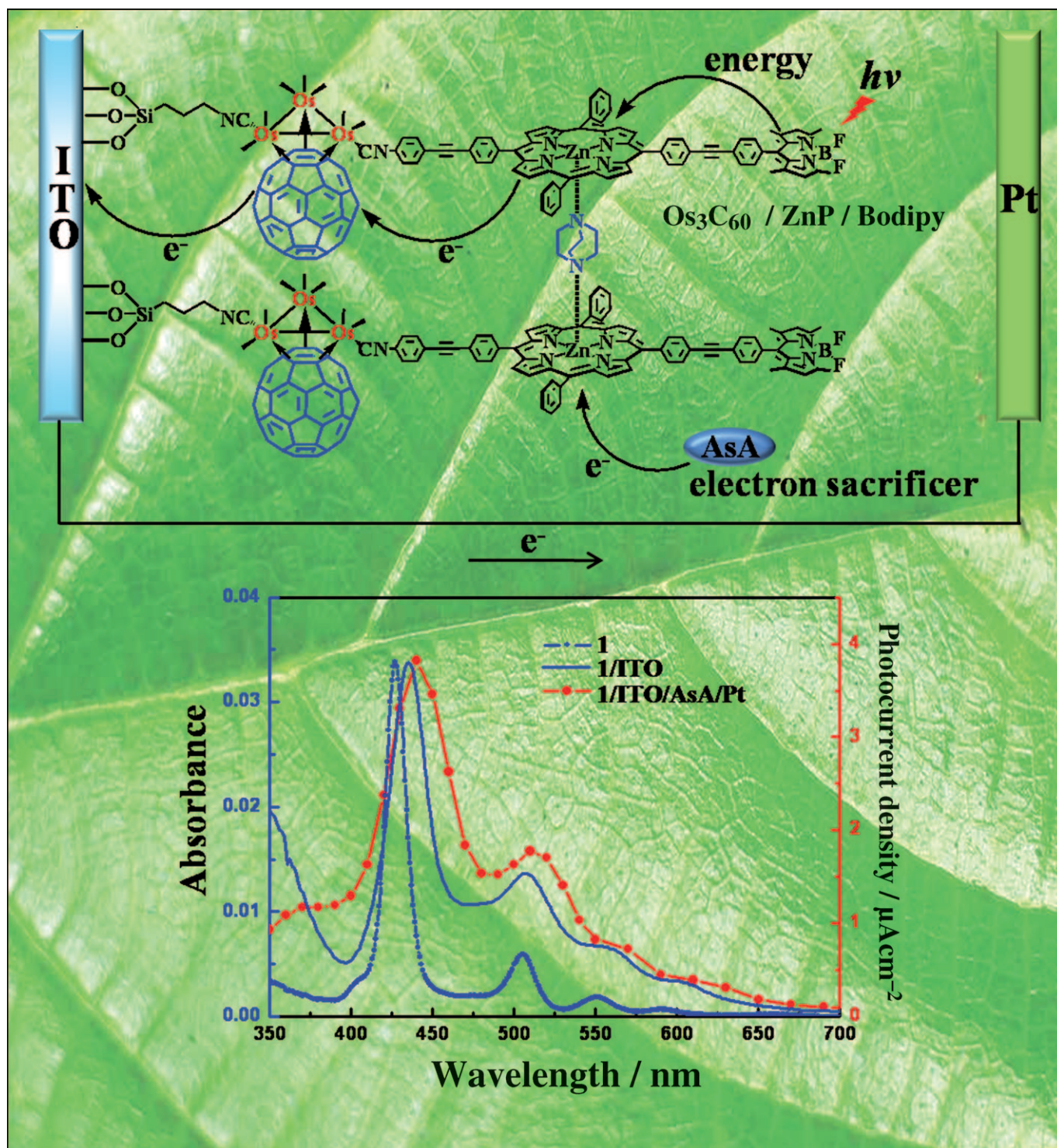


Remarkably Efficient Photocurrent Generation Based on a [60]Fullerene–Triosmium Cluster/Zn–Porphyrin/Boron–Dipyrin Triad SAM

Chang Yeon Lee,^[a] Jae Kwon Jang,^[a] Chul Hoon Kim,^[b] Jaehoon Jung,^[c]
Bo Keun Park,^[a] Jihee Park,^[d] Wonyong Choi,^[d] Young-Kyu Han,^{*,[c]} Taiha Joo,^{*,[b]} and
Joon T. Park^{*,[a]}



Abstract: A new artificial photosynthetic triad array, a [60]fullerene–triosmium cluster/zinc–porphyrin/boron–dipyrrin complex (**1**, Os₃C₆₀/ZnP/Bodipy), has been prepared by decarbonylation of Os₃(CO)₈(CN(CH₂)₃Si(OEt)₃)(μ₃-η²:η²:η²-C₆₀) (**6**) with Me₃NO/MeCN and subsequent reaction with the isocyanide ligand CNZnP/Bodipy (**5**) containing zinc porphyrin (ZnP) and boron dipyrrin (Bodipy) moieties. Triad **1** has been characterized by various spectroscopic methods (MS, NMR, IR, UV/Vis, photoluminescence, and transient absorption spectroscopy). The electrochemical properties of **1** in chlorobenzene (CB) have been examined by cyclic voltammetry; the general feature of the cyclic voltammogram of **1** is nine

reversible one-electron redox couples, that is, the sum of those of **5** and **6**. DFT has been applied to study the molecular and electronic structures of **1**. On the basis of fluorescence-lifetime measurements and transient absorption spectroscopic data, **1** undergoes an efficient energy transfer from Bodipy to ZnP and a fast electron transfer from ZnP to C₆₀; the detailed kinetics involved in both events have been elucidated. The SAM of triad **1** (1/ITO; ITO = indium–tin oxide) has been prepared by immersion of an ITO electrode in a CB solution of **1** and diaza-

bicyclo-octane (2:1 equiv), and characterized by UV/Vis absorption spectroscopy, water contact angle, X-ray photoelectron spectroscopy, and cyclic voltammetry. The photoelectrochemical properties of **1**/ITO have been investigated by a standard three-electrode system in the presence of an ascorbic acid sacrificial electron donor. The quantum yield of the photoelectrochemical cell has been estimated to be 29% based on the number of photons absorbed by the chromophores. Our triad **1** is unique when compared to previously reported photoinduced electron-transfer arrays, in that C₆₀ is linked by π bonding with little perturbation of the C₆₀ electron delocalization.

Keywords: electron transfer • monolayers • photoelectrochemistry • self-assembly • triads

Introduction

Photoinduced electron transfer (PET) in donor–acceptor (D–A) molecular systems continues to receive considerable attention for potential applications such as optoelectronics, photonics, sensors, and other advanced nanostructured devices.^[1] Recent progress in [60]fullerene functionalization has led to the development of spectacular surface-immobilized molecular architectures on a wide variety of surfaces and, in particular, to highly successful application of the prominent artificial photovoltaic devices by design of integrated, multi-

component, photosynthetic model systems to transmit and process solar energy.^[2] Functionalized C₆₀ molecular systems for PET processes often consist of electron donors such as porphyrin,^[4] ferrocene,^[5] thiophene,^[6] and carbon nanotubes^[7] with additional light-harvesting antenna molecules. C₆₀ functions as an efficient acceptor because of its intriguing characteristics that allow acceleration of photoinduced charge separation and slowing down of charge recombination in the electron-transfer process. This is mainly due to its relatively low-lying LUMO and small reorganization energy.^[4c] Various molecular arrays containing D–A sites and antenna molecules, from dyads to hexads, have been prepared to address the detailed kinetics of energy and electron transfer and, in a few cases, these have been successfully applied to solar energy conversion.^[8] Fullerene–porphyrin architectures for photosynthetic antenna and reaction center models have been reviewed by Guldi.^[9] D'Souza and co-workers have recently reported a fullerene/zinc–porphyrin/boron–dipyrrin triad based on self-assembled supramolecular methodology, which has revealed photoinduced sequential energy and electron transfers among the triad components.^[10] Imahori and co-workers have reported extremely long-lived charge-separated states of 380 or 530 ms in tetrad^[8c] and pentad^[8d] systems containing ferrocene, porphyrin, and fullerene. These systems involve a cascade of photoinduced energy transfers and multistep electron transfers within the molecular arrays and mimic natural photosynthetic reaction systems.

SAMs are highly ordered molecular assemblies that form spontaneously by chemisorption of linkage-functionalized molecules onto surfaces and by lateral intermolecular van der Waals interactions.^[11] SAMs and multilayer thin films with potential gradients have shown promise in imitating

[a] Dr. C. Y. Lee,⁺ J. K. Jang,⁺ Dr. B. K. Park, Prof. J. T. Park
Department of Chemistry and School of Molecular Science
Korea Advanced Institute of Science and Technology
Daejeon, 305-701 (Korea)
Fax: (+82) 42-350-5826
E-mail: joontpark@kaist.ac.kr

[b] Dr. C. H. Kim, Prof. T. Joo
Department of Chemistry
Pohang University of Science and Technology
Pohang 790-784 (Korea)
Fax: (+82) 54-279-8127
E-mail: thjoo@postech.ac.kr

[c] J. Jung, Dr. Y.-K. Han
Computational Chemistry Laboratory, Corporate R&D
LG Chem Ltd Research Park, Daejeon, 305-380 (Korea)
Fax: (+82) 42-865-3160
E-mail: ykhan@kbsi.re.kr

[d] J. Park, Prof. W. Choi
School of Environmental Science and Engineering
Pohang University of Science and Technology
Pohang 790-784 (Korea)

[⁺] These authors contributed equally to this work.

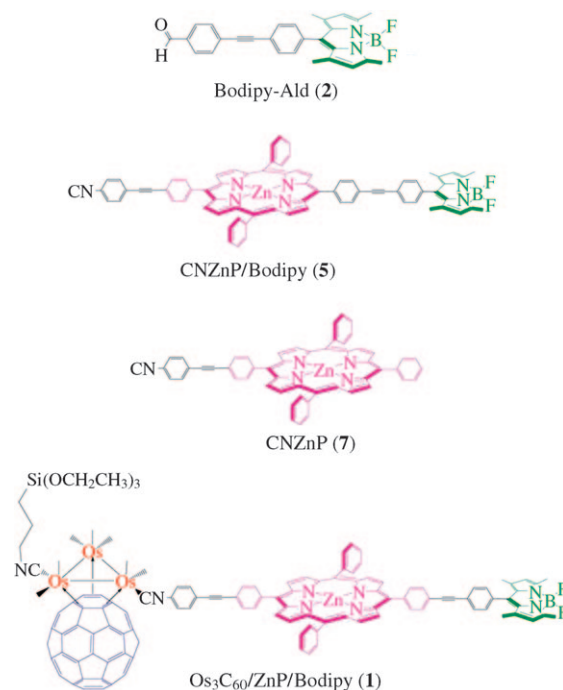
Supporting information for this article is available on the WWW under <http://dx.doi.org/10.1002/chem.201000215>.

natural photosynthetic systems and in fabricating efficient and well-defined photovoltaic cells. A variety of SAMs, including porphyrin/fullerene,^[2a,b] a ferrocene/porphyrin/fullerene triad,^[2c,d] a ferrocene/porphyrin/fullerene/boron-dipyrrin tetrad,^[2e] and organometallic fullerene^[2j] on gold and indium–tin oxide (ITO) surfaces have previously been studied with respect to solar energy conversion. A comprehensive review of the chemistry of supramolecular [60]fullerene on surfaces has appeared recently.^[3] However, there have been few studies devoted to a detailed examination of photoinduced energy and electron transfers in these artificial photovoltaic devices.

In our previous work, we described a highly ordered [60]fullerene triosmium cluster–zinc–porphyrin dyad SAM on an ITO surface^[12] that achieved nearly full coverage with the aid of diazabicyclooctane (DABCO). This system exhibited the highest photocurrent generation efficiency, at 19.5%, that had been reported for dyad photoelectrochemical cells based on SAMs. Our C₆₀–metal cluster complexes are unique in that the C₆₀–metal interaction in μ₃–η²:η²:η²–C₆₀ bonding mode perturbs the C₆₀ hybridization very little, as shown by our SAM, photovoltaic cell application, and X-ray structural characterization evidence. These earlier studies also revealed remarkable thermal and electrochemical stabilities and electronic communication between C₆₀ and metal cluster centers, which proved uniquely suitable for various electronic device applications.

Imahori and co-workers have described an extremely high quantum yield (50%) photoelectrochemical cell that uses a mixed SAM composed of a boron dipyrroin moiety and a ferrocene/porphyrin/fullerene triad.^[2e] The boron dipyrroin (Bodipy; 4,4-difluoro-4-bora-3a,4a-diaza-*s*-indacene) molecule has often been employed as an antenna light-harvesting molecule because it has many favorable properties such as high fluorescence quantum yield, low rates of intersystem crossing, large molar absorption coefficients, long excited-state lifetimes, and excellent photostability.^[13] Its structures can also be tailored by a variety of substitutions to tune its fluorescence characteristic, allowing the development of applications in the fields of biological labeling,^[14] molecular wires,^[15] and artificial photosynthetic systems.^[2e]

In this study, we report full details of the preparation and characterization of a new triad artificial photosynthetic molecule, [60]fullerene–triosmium cluster/zinc–porphyrin/boron–dipyrrin (**1**, Os₃C₆₀/ZnP/Bodipy), and describe its application to a photoelectrochemical cell based on a SAM of **1** with DABCO on an ITO electrode (**1**/ITO). Our triad **1** is unique compared with the previously reported PET arrays, in that the C₆₀ cage is linked through π bonding. Complexation between **1** and DABCO in solution has been monitored by ¹H NMR spectroscopy. DFT has been used to study the molecular and electronic structures of **1**. The detailed kinetics of energy and electron transfer have been investigated by fluorescence-lifetime measurements and transient absorption (TA) spectroscopy. Structures of the title molecule (**1**) and other related key compounds (**2**, **5**, and **7**) are depicted in Scheme 1.

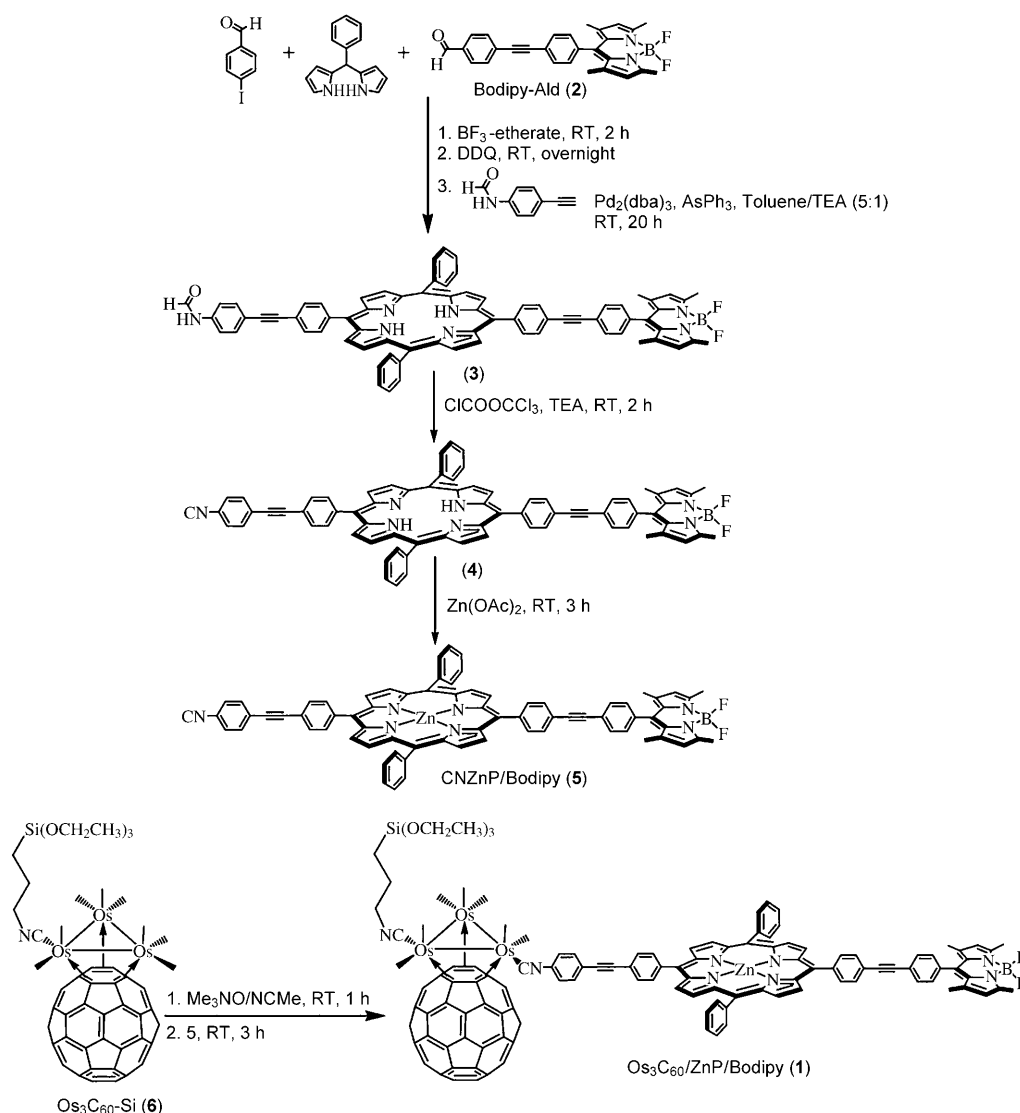


Scheme 1. Structures of **1**, **2**, **5**, and **7**.

Results and Discussion

Synthesis and characterization of 1–7: The synthetic routes to **1** are summarized in Scheme 2. Compound **2** (Bodipy-Ald) was prepared in 87% yield by a published procedure, as described in the Experimental Section. The key synthetic intermediate **3** was prepared in 8% yield from a mixed condensation of the *meso*-phenyldipyrromethane, 4-iodobenzaldehyde, and Bodipy-Ald (**2**) in the presence of BF₃–diethyl etherate, followed by an in situ Pd-mediated coupling of crude porphyrin mixtures with *N*-(4-ethynylphenyl)formamide. Dehydration of **3** by diphosgene afforded isocyanide-functionalized compound **4** in 75% yield. Metallation of **4** with Zn(OAc)₂ produced compound **5** in 87% yield. Decarbonylation of Os₃(CO)₈(CN(CH₂)₃Si(OEt)₃)(μ₃–η²:η²:η²–C₆₀) (**6**) with Me₃NO/MeCN, followed by treatment with **5** in chlorobenzene (CB) at room temperature, gave triad **1** in 35% yield.

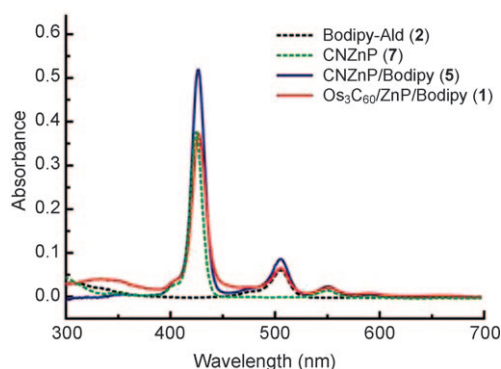
Compounds **2–5**, were characterized by NMR (¹H, ¹¹B, and ¹⁹F), IR, and MALDI-TOF mass spectroscopy, and by elemental analyses. Formulation of triad **1** is based on the molecular ion isotope multiplets (*m/z* (highest peak): 2868) in the MALDI-TOF mass spectrum and on spectroscopic and microanalytical data. The IR spectrum of **1** exhibits two NC stretches: one at 2187 cm^{−1}, due to the silyl-substituted isocyanide ligand; and one at 2139 cm^{−1}, due to the porphyrin-substituted isocyanide ligand **5**. An essentially identical CO stretching pattern to that seen for the structurally characterized 1,2-*cis,trans*-disubstituted Os₃(CO)₇–(CNCH₂Ph)₂(μ₃–η²:η²:η²–C₆₀) (**8**)^[16] complex was observed, which implies that the structure of **1** is isomorphous with that of **8** (see Figure S1 in the Supporting Information). The

Scheme 2. The synthetic routes to **1**.

shift of the terminal CO stretching bands of **1** to the low-energy region by approximately 20 cm^{-1} compared with those of **6** reflects an additional electron-donor effect of the isocyanide ligand **5**. The ^{11}B NMR spectra of **1–5** reveal a triplet resonance for each at 0.40, 0.39, -0.46 , 0.44, and -0.44 ppm, respectively. These are due to a single boron atom coupled to the two equivalent fluorine atoms in **1–5**. The ^{19}F NMR spectra of **1–5** exhibit a quartet resonance for each at -146.7 , -146.7 , -146.7 , -146.7 , and -149.3 ppm, respectively. These are due to the two equivalent fluorine atoms coupled to a boron atom in these compounds. All ^1H NMR spectral data for **1–5** and **7** are consistent with the corresponding structures shown in Schemes 1 and 2

Steady-state absorption and fluorescence spectroscopy of 1, 2, 5, and 7: The UV/Vis spectrum of **1** in CB (Figure 1) exhibits characteristic absorption bands for ZnP (Soret band: $\lambda_{\text{max}}=427\text{ nm}$; Q bands: $\lambda_{\text{max}}=550, 590\text{ nm}$), Bodipy ($\lambda_{\text{max}}=$

505 nm), and C_{60} ($\lambda_{\text{max}}=350\text{ nm}$). The spectra of reference compounds **2** and **7** show absorptions due to Bodipy and ZnP, respectively. The spectrum of reference compound **5** is

Figure 1. UV/Vis absorption spectra of **1**, **2**, **5**, and **7** in CB.

essentially a sum of the two absorption spectra of **2** and **7**, as expected. The absorption band of Bodipy does not overlap that of the ZnP or the C₆₀ moiety, indicating that Bodipy can be excited selectively in **1** and **5**.

The steady-state fluorescence emission spectra of **1** and **5** are provided in Figure 2a. Bodipy excitation of **5** at 505 nm results in a typical Bodipy fluorescence with an emission

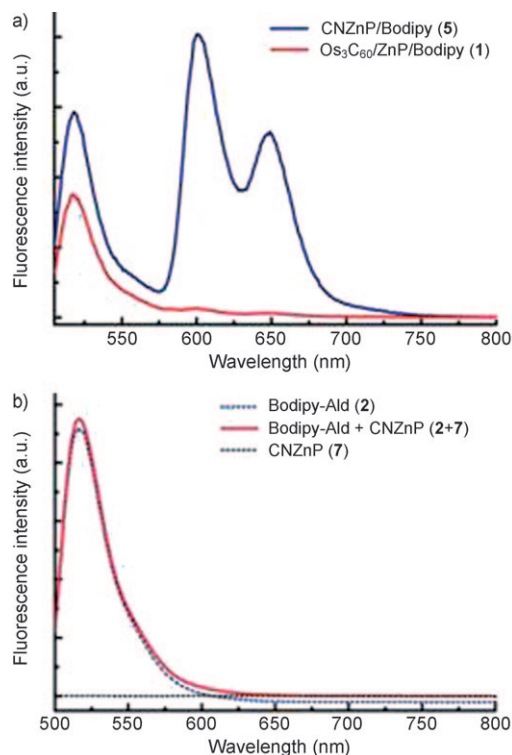


Figure 2. a) Steady-state fluorescence spectra of **1** and **5** in CB. b) Steady-state fluorescence spectra of **2**, **7**, and a 1:1 mixture of **2** and **7** in CB. The concentration (0.8 μM) was kept constant for each of the species. Samples were excited at 505 nm.

maximum at 518 nm, along with ZnP emissions at 601 and 649 nm, implying that a definite intramolecular energy transfer takes place from Bodipy to ZnP in **5**. To address the nature of this energy transfer, fluorescence measurements were performed for **2**, **7**, and a 1:1 mixture of **2** and **7** (Figure 2b). Excitation of **2** at 505 nm reveals a Bodipy emission, whereas that of **7** shows no emission, which indicates that ZnP is not excited by radiation at 505 nm. Furthermore, excitation of a 1:1 mixture of **2** and **7** at 505 nm gives a simple sum of the emission spectra of **2** and **7**, indicating no intermolecular energy transfer from **2** to **7**; this observation agrees with studies reported earlier.^[10] However, when triad **1** is excited at 505 nm, ZnP emission is quenched by over 96% compared with that of **5** (Figure 2a). There is no appreciable C₆₀ emission in the 700–750 nm range, so these results show clearly that an efficient electron transfer occurs from ZnP to C₆₀ in **1**. Overall, triad **1** undergoes an energy transfer from Bodipy to ZnP and an electron transfer from ZnP to C₆₀.

Electrochemistry of 1, 2, 5, 6, and 7: The electrochemical properties of free C₆₀, **1**, **2**, **5**, **6**, and **7** have been examined by cyclic voltammetry in CB solutions, with tetrabutylammonium perchlorate as the supporting electrolyte (Figure 3) and the corresponding half-wave potentials ($E_{1/2}$) are summarized in Table 1.

The data for free C₆₀ are included for comparison. Compounds **2** and **7** show a reversible one-electron redox wave at $E_{1/2} = -1.70$ V and four reversible one-electron redox waves at $E_{1/2} = 0.65, 0.33, -1.87,$ and -2.17 V, respectively, which are attributed to redox reactions at Bodipy and ZnP centers. The cyclic voltammogram (CV) of **5** is the sum of those of **2** and **7**, as expected, with redox waves at $E_{1/2} = 0.64, 0.32, -1.68, -1.87,$ and -2.08 V. The CV of **6** reveals four reversible one-electron redox waves, with the third and fourth waves overlapping. These have been observed similarly in various known complexes, including Os₃(CO)₈-(PMe₃)(μ₃-η²:η²:η²-C₆₀)¹⁷ and Os₃(CO)_{9-n}(CNCH₂Ph)_n(μ₃-η²:η²:η²-C₆₀) ($n = 2, 3,$ and 4),^[16] due to C₆₀ reductions combined with electronic communication between the C₆₀ and the metal-cluster centers. The general feature of the CV of **1** is again the sum of those of **5** and **6**, as expected. It shows nine reversible one-electron redox couples with the sixth, seventh, and eighth waves overlapping. On the basis of these observations, the nature of each redox wave of triad **1** is assigned unambiguously in Figure 3 and in Table 1. The first and second redox waves at $E_{1/2} = 0.51$ and 0.34 V correspond to the redox reactions of ZnP^{1+/2+} and ZnP^{0/1+}, respectively. The third and fourth redox waves at $E_{1/2} = -1.09$ and -1.43 V are due to the redox reaction of C₆₀^{0/1-} and C₆₀^{1-/2-}, respectively. The fifth couple at $E_{1/2} = -1.69$ V is attributed to the redox reaction of Bodipy^{0/1-}. The sixth to eighth waves at $E_{1/2} = -1.82, -1.82,$ and -1.90 V overlap, and correspond to C₆₀^{2-/3-}, C₆₀^{3-/4-}, and ZnP^{0/1-}, respectively. The ninth redox wave for ZnP^{1-/2-} appears at $E_{1/2} = -2.12$ V.

The molecular and electronic structures of **1** have been studied by applying DFT using the BPW91 functional. Figure 4 displays the optimized structure, the HOMO, and the LUMO. The two isocyanide ligands are coordinated in a *cis,trans* fashion on the triosmium cluster. The triosmium triangle, ZnP, and Bodipy moieties are almost coplanar and perpendicular to the four coplanar phenyl rings in the spacer. The majority of the HOMO is located on the ZnP moiety, whereas the LUMO is found to be entirely on the C₆₀ moiety.

Time-resolved fluorescence spectroscopy of 1, 2, 5, and 7:

To investigate the kinetics of the energy and electron transfers in triad **1**, time-resolved fluorescence (TRF) studies for **1**, **2**, **5**, and **7** were performed by time-correlated single-photon counting and fluorescence up-conversion methods. Multiexponential fit results for all the TRF signals are summarized in Table 2.

TRF of Bodipy (**2**) or of ZnP (**7**) alone displays single-exponential decay, to give the S₁ state lifetime of 1.9 or 1.8 ns, respectively (Figure S2 in the Supporting Information). When the Bodipy moieties in **5** and **1** are excited by 500 nm

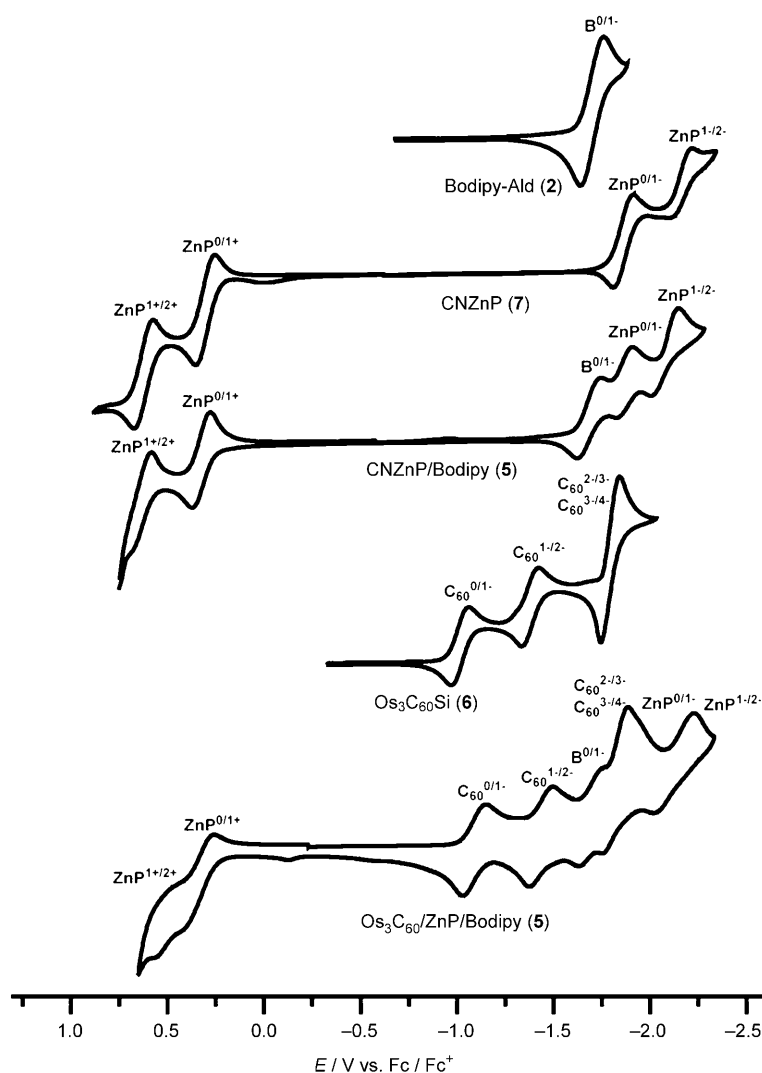


Figure 3. CVs of **1**, **2**, **5**, **6**, and **7** in dry deoxygenated CB (supporting electrolyte 0.1 M [(*n*Bu)₄N][ClO₄]; scan rate 10 mV s⁻¹).

Table 1. Half-wave potentials ($E_{1/2}$ vs. $E_{\text{Fc}^0/\text{Fc}^+}$) of C₆₀, **1**, **2**, **5**, **6**, and **7** in CB.

Compound	ZnP ^{1+/2+}	ZnP ^{0/1+}	C ₆₀ ^{0/1-}	C ₆₀ ^{1-/2-}	B ^{0/1-}	C ₆₀ ^{2-/3-}	C ₆₀ ^{3-/4-}	ZnP ^{0/1-}	ZnP ^{1-/2-}
C ₆₀ ^[a]	–	–	-1.06	-1.43	–	-1.91	-2.38	–	–
2 ^[b]	–	–	–	–	-1.70	–	–	–	–
7 ^[b]	0.65	0.33	–	–	–	–	–	-1.87	-2.17
5 ^[b]	0.64	0.32	–	–	-1.68	–	–	-1.87	-2.08
6 ^[b,c]	–	–	-1.05	-1.41	–	-1.84	–	–	–
1 ^[b]	0.51	0.34	-1.09	-1.43	-1.69	-1.82	–	-1.90	-2.12

[a] See reference [17]. [b] This work. [c] See reference [24].

pulses, much faster decays of the Bodipy emission at 525 nm, and the corresponding rises of the Q-band emission of ZnP at 650 nm, are observed (Figure 5). This observation clearly demonstrates the occurrence of photoinduced energy transfer from the Bodipy to ZnP moieties in **5** and **1**. The energy-transfer time constants are 31 and 41 ps in **5** and **1**, respectively. Direct excitation of the ZnP moiety in **5** by

550 nm pulses leads to a slow 1.6 ns single-exponential decay, without a rise component for the ZnP emission, which supports the assumption that the 23 ps rise component is due to energy transfer. The 1.6 ns lifetime of the ZnP moiety in **5** matches well with the lifetime of 1.8 ns found in **7**.

In contrast to **5**, TRF of the ZnP in the triad **1** shows a fast decay in 35–50 ps, indicating a fast electron transfer from ZnP to C₆₀ as confirmed by TA spectroscopy (see below). Interestingly, the electron-transfer rate in triad **1** is somewhat dependent on the excitation wavelength, as shown in Table 2. The small slow-decay components (τ_3) comprising about 1% of the total decay may be due to an impurity and/or to the triad in a conformation that is not favorable for charge transfer. Free-energy changes of **1** and **5** for charge recombination (CR), charge separation (CS), and energy transfer (ENT) in CB were calculated by using Weller equations.^[18] The center-to-center distance (R_{CC}) between ZnP and C₆₀ moieties in the Weller equation is calculated to be 21 Å from the optimized structure (see above). These results are summarized in Table 3, as are the calculated rate constants for CR, CS, and ENT processes. The magnitudes of rate constants of **1** and **5** for CS and ENT are comparable to the values reported for other similar artificial photosynthetic systems.^[4] Energy levels, ENT, electron-transfer (ET), and relaxation processes of **1** are summarized schematically in Figure 6.

Transient absorption spectroscopy: TA spectra of **1** were measured to verify the formation of the charge-separated states in triad **1** (Figure 7). They show a negative peak at 525 nm at an early stage due to the stimulated emission of the Bodipy S₁ state. More importantly, photoinduced absorption develops immediately after the excitation over the

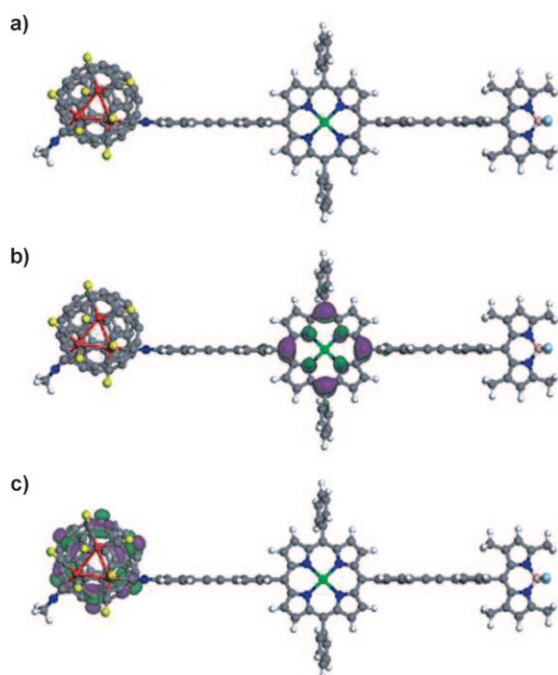


Figure 4. Compound **1**: a) Optimized structure; b) HOMO; c) LUMO.

Table 2. Multiexponential fit for the TRF of **1**, **2**, **5**, and **7** in CB detected at the Bodipy (525 nm) and ZnP (650 nm) emission wavelengths.^[a]

Compound	λ_{ex} [nm]	Bodipy (525 nm)		ZnP (650 nm)		
		τ_1 [ps]	τ_1 [ps]	τ_2 [ps]	τ_3 [ns]	
2	500	1900	–	–	–	–
7	550	–	–	–	–	1.8
5	500	31	–23	–	–	1.6
	550	–	–	–	–	1.6
1	500	41	–31	50 (99.4)	–	1.6 (0.6)
	550	–	–	35 (98.7)	–	0.94 (1.3)

[a] A negative time constant indicates a rise. Values in parentheses are relative amplitudes [%].

whole detection wavelength region, and it increases gradually to 500 ps. It is well known that charge separation and recombination dynamics can be monitored directly by probing the ZnP radical cation (ZnP^+) and the C_{60} radical anion (C_{60}^-), which show transient absorption bands centered at approximately 650 and 1000 nm, respectively.^[4c,e,h] Unfortunately, however, the S_1 state of ZnP is also known to absorb strongly near the same wavelength region.^[19] The TAs of Bodipy (**2**) and ZnP (**7**) (Figures S3 and S4, respectively, in the Supporting Information) show clearly that both absorb strongly in the same wavelength region. The lifetimes of the Bodipy and ZnP moieties in **1** are 41 and 50 ps, respectively, and, therefore, the photoinduced absorptions can be safely assigned within approximately 50 ps to the excited-state absorptions of the S_1 states of Bodipy and ZnP. The photoinduced absorptions in the visible and near-infrared (NIR) regions, which show a slow increase of up to 500 ps, should then be assigned to the ZnP^+ and C_{60}^- species, respectively.

The charge separation and recombination kinetics in triad **1** were investigated by TA at single detection wavelengths.

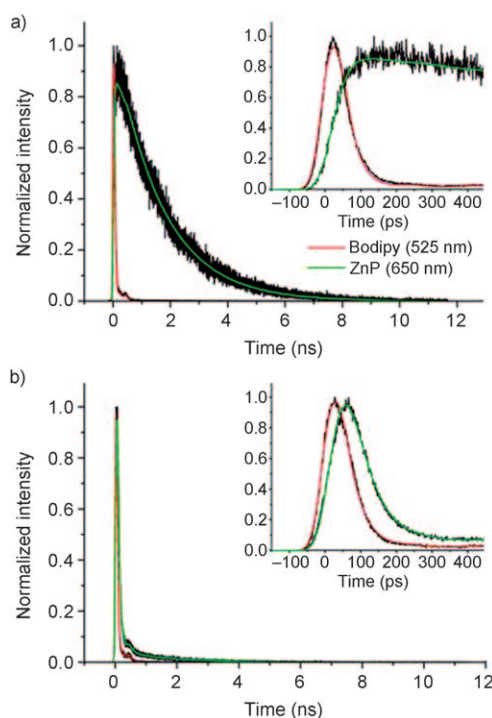


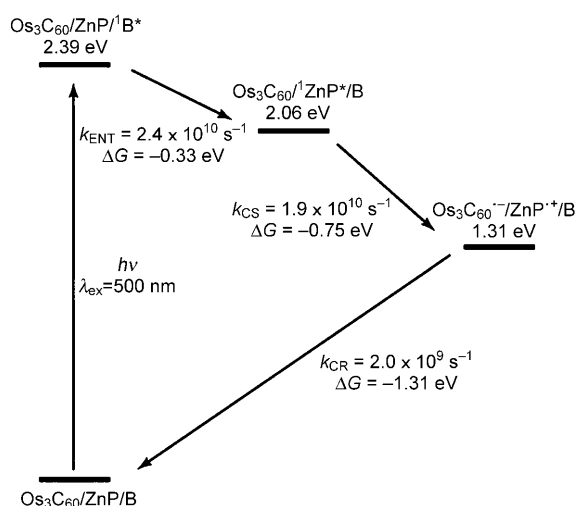
Figure 5. Time-resolved fluorescence signals measured at 525 nm and 650 nm in CB for a) **5** and b) **1**. Insets: TRF signals at early times (excitation wavelength 500 nm).

Table 3. Energy and electron-transfer rate constants and free-energy changes of **1** and **5** in CB.

Compound	$\Delta G_{\text{ENT}}^{\text{[a]}}$ [eV]	$k_{\text{ENT}}^{\text{[b]}}$ [s^{-1}]	$\Delta G_{\text{CS}}^{\text{[a]}}$ [eV]	$k_{\text{CS}}^{\text{[b]}}$ [s^{-1}]	$\Delta G_{\text{CR}}^{\text{[a]}}$ [eV]	$k_{\text{CR}}^{\text{[b]}}$ [s^{-1}]
5	–0.33	3.1×10^{10}	–	–	–	–
1	–0.33	2.4×10^{10}	–0.75	1.9×10^{10}	–1.31	2.9×10^9

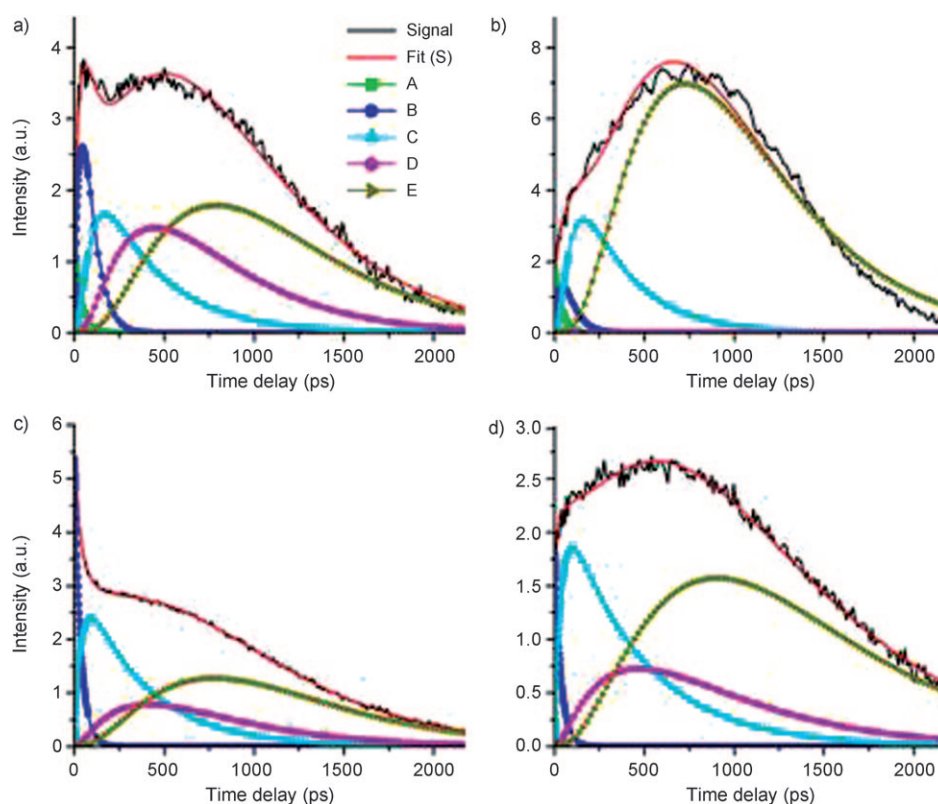
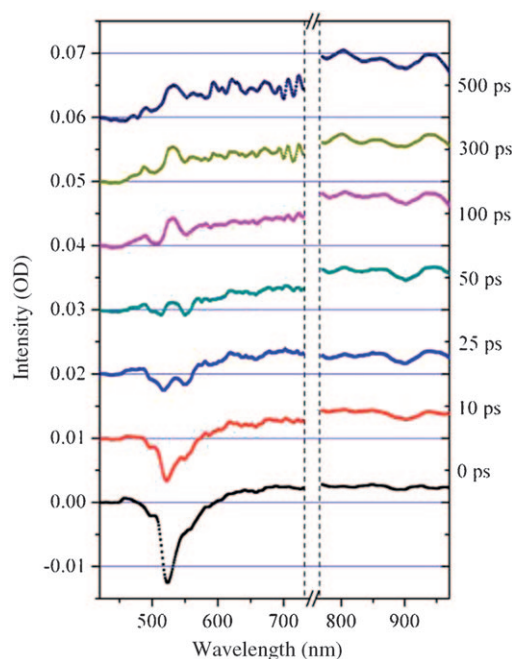
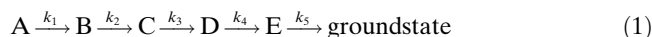
[a] ΔG_{ENT} is the energy difference between the excited singlet state of Bodipy and that of ZnP in **1** and **5**. The ΔG_{CS} and ΔG_{CR} values of **1** are calculated from the Weller equations ($\Delta G_{\text{CS}} = E_{\text{ox}}(\text{ZnP}) - E_{\text{red}}(\text{C}_{60}) - E_0 - E_c$ and $\Delta G_{\text{CR}} = E_{\text{red}}(\text{C}_{60}) - E_{\text{ox}}(\text{ZnP}) - E_c$). E_{ox} and E_{red} are ZnP^{ox} (0.34 V) and $\text{C}_{60}^{\text{red}}$ (1.09 V), respectively. E_0 is the energy of the 0–0 transition between the lowest excited state and ground state of ZnP. E_c (coulombic energy) is calculated as $e^2/(4\pi\epsilon_0\epsilon_s R_{\text{cc}})$, in which R_{cc} is the center-to-center distance between ZnP and C_{60} in **1** and ϵ_s is the dielectric constant of the solvent (5.7 for CB). [b] Rate constants for ENT, CS, and CR are calculated from the equations: $k_{\text{ENT}}(\mathbf{5}) = \tau_{(\text{CNZnP-Bodipy}^*)}^{-1} - \tau_{(\text{Bodipy-Ald}^*)}^{-1}$, $k_{\text{ENT}}(\mathbf{1}) = \tau_{(\text{Os}_3\text{C}_{60}/\text{ZnP/Bodipy}^*)}^{-1} - \tau_{(\text{Bodipy-Ald}^*)}^{-1}$, $k_{\text{CS}} = \tau_{(\text{Os}_3\text{C}_{60}/\text{ZnP}^*/\text{Bodipy}^*)}^{-1} - \tau_{(\text{CNZnP}^*)}^{-1}$, and $k_{\text{CR}} = \tau_{(\text{Os}_3\text{C}_{60}/\text{ZnP}^*/\text{Bodipy}^*)}^{-1}$.

Figure 8 shows the TA signals of **1**, in which Bodipy and ZnP moieties are excited by 500 and 550 nm pulses, respectively, and the subsequent transient species are probed at two different wavelengths, 650 and 1000 nm. Note that all the monomer moieties included in triad **1** show strong excited-state absorptions at both detection wavelengths. To describe the TA signals properly, a kinetic scheme that includes all the chemically and spectroscopically distinct species needs to be considered. To check the possibility that the excited state of the fullerene moiety (C_{60}^*) is generated, we measured the TRF signal at 720 nm (Figure S5 in the Supporting Information) at which the C_{60}^* emits.^[4e,20] We did

Figure 6. Energy levels, ENT, ET, and relaxation processes of **1**.

not observe any decay component that may be responsible for the C_{60}^* emission when the Bodipy (500 nm) or the ZnP Q band (550 nm) is excited. In fact, the TRF signal was almost the same as the Q-band emission at 650 nm, which indicates that the possibility of the generation of the charge-separated products from the C_{60}^* , and a kinetic scheme involving the C_{60}^* can be ignored. Most of the charge-separated products should, therefore, be generated from the singlet excited state of ZnP. Any contribution of the unreactive ZnP can be ignored because of its negligible amplitude in the TRF measurement. All the TA signals in Figure 8 have been fitted by the global fitting method. They, and especially those probed at 1000 nm, show a prominent rise that is much slower than the lifetime of the S_1 state of ZnP, which clearly requires an intermediate before the charge-separated state undergoes the charge recombination process.

We have included two such intermediate charge-separated states to fit all the TA data satisfactorily. Thus, energy transfer, charge separation, and recombination reaction schemes can be proposed as in [Eq. (1)], in which A is $Os_3C_{60}/ZnP/Bodipy^*$, B is $Os_3C_{60}/ZnP^*/Bodipy$, and C is $Os_3C_{60}^{(-)}/ZnP^{(+)}/Bodipy$. D and E can be regarded as the charge-separated states before the charge-recombination process.

Figure 8. Transient absorption signal of **1** in CB. Excitation and probe wavelengths (nm): a) 500, 650; b) 500, 1000; c) 550, 650; d) 550, 1000, respectively.Figure 7. Transient absorption spectra of the triad **1** in CB (excitation wavelength 500 nm). Each curve is displaced by 0.01 OD (OD = optical density) from the preceding curve.

D and E are introduced to represent the conformational and other relaxation processes of the nascent charge-separated state C, before it undergoes the charge recombination process, and they may not represent distinct chemical species. Thus, k_5 should be the charge recombination rate. The rate equations for each component can be expressed by the matrix given in [Eq. (2)].

$$\frac{d}{dt} \begin{pmatrix} [A(t)] \\ [B(t)] \\ [C(t)] \\ [D(t)] \\ [E(t)] \end{pmatrix} = \begin{pmatrix} -k_1 & 0 & 0 & 0 & 0 \\ k_1 & -k_2 & 0 & 0 & 0 \\ 0 & k_2 & -k_3 & 0 & 0 \\ 0 & 0 & k_3 & -k_4 & 0 \\ 0 & 0 & 0 & k_4 & -k_5 \end{pmatrix} \begin{pmatrix} [A(t)] \\ [B(t)] \\ [C(t)] \\ [D(t)] \\ [E(t)] \end{pmatrix} \quad (2)$$

A complete set of rate equations from [A(t)] to [E(t)] can be solved from [Eq. (2)] by using the determinant method.^[21] All the transient absorption signals are fitted with a model function [Eq. (3)], in which X_m denotes a relative amplitude for each $X(t)$.

$$S = \sum_{X=A-E} X_m [X(t)] \quad (3)$$

In the fitting procedure, the initial concentration is constrained to $[A]_0=1$ or $[B]_0=1$, depending on the excitation wavelength, and k_1 and k_2 are fixed to the values obtained from the TRF measurements. The fit results were overlaid with the experimental curve in Figure 8, and the amplitude of each component (X_m) and the rate constants are listed in Table 4. When the intermediates D and E are not included

Table 4. Fitted amplitudes and rate constants for the transient absorption signals of triad **1** in chlorobenzene.^[a]

λ_{ex} [nm]	λ_{probe} [nm]	k_1^{-1} [ps]	k_2^{-1} [ps]	k_3^{-1} [ps]	k_4^{-1} [ps]	k_5^{-1} [ps]
500	650	41 (6)	50 (31)	350 (12)	340 (20)	350 (31)
	1000	41 (5)	50 (10)	290 (15)	310 (≈ 0)	340 (71)
550	650	–	35 (35)	350 (20)	400 (13)	370 (32)
	1000	–	35 (15)	430 (20)	430 (17)	440 (48)

[a] Values in parentheses are relative amplitudes [%].

in the model, the fitting is not satisfactory because the slow rise component of about 400 ps shown in all the TA signals cannot be described by a three- or four-step model. Hence, inclusion of the relaxation processes of the nascent charge-separated state is required, and they may change the absorption spectrum of the charge-separated state. Note that the nascent charge-separated state formed from the singlet excited state of ZnP may be in a vibrationally excited state, which may undergo vibrational relaxation. This process can be ignored, however, because the vibrational relaxation occurs in a few tens of picoseconds, much faster than the observed 400 ps.^[22] Conformational dynamics such as the twisting and bending motions around the chromophores in the

excited state could be one of the possible candidates responsible for the relaxation, because the 400 ps timescale may correspond to the slow structural changes. Although the conformational dynamics in the ground state may not be feasible in our triad system owing to the rigid structure, the conformational dynamics in the excited state may become possible because the conjugation in the excited state is much weaker than that in the ground state. Further studies are needed to identify the origin of the species D and E, which are beyond the scope of this work.

All the TA signals follow the proposed reaction scheme qualitatively. The relative contribution of each component to the TA signal shows a dependence on the excitation wavelength. When Bodipy is excited, the contribution of the ZnP absorption is higher than that of the charge-separated products (C, D, and E), whereas when the Q band of ZnP is excited, this is reversed, indicating that charge-separation dynamics and subsequent relaxation processes depend substantially on the energetics between the Q band of ZnP and C_{60} . Although chemical properties of the charge-separated intermediates C, D, and E, as well as the kinetics between these species, have not been identified, the decay rate (k_5) of E may correspond directly to the charge-recombination process.

Compared to the results of recent TA experiments for similar dyad and triad systems,^[10,4h] charge recombination kinetics with a time constant of about 350–400 ps seem to be quite fast, although similar experimental results for the dyads were reported in picosecond TA experiments by Imahori and co-workers.^[4c] D'Souza et al. reported a charge-recombination time of 5 ns in a supramolecular triad in *o*-dichlorobenzene,^[10] although this value has a large uncertainty because a flash-photolysis technique with nanosecond time resolution was employed. In contrast, Schuster et al. reported time constants in the range 145–435 ns for an azobenzene-linked dyad in tetrahydrofuran.^[4h] However, they also reported dramatically decreased lifetimes in the range 600 ps–1.2 ns for the same sample in benzonitrile. Therefore, if we consider that the kinetics of the recombination process may be highly solvent-dependent, our results are quite similar to the results for these systems. Our system may possibly show slower recombination rates in other polar solvents, such as tetrahydrofuran.

Interaction of **1 with DABCO:** To elucidate the interaction of **1** with DABCO, the complexation between **1** and DABCO in solution was monitored by ¹H NMR spectroscopy (Figure 9). When DABCO (0.5 equiv) was added to a solution of **1** in chloroform (5.5 mM) two resonances in a 1:1 ratio at –1.88 and –4.61 ppm, shifted upfield relative to free DABCO at 2.80 ppm, were observed. These were due to the six inner methylene hydrogen atoms (denoted by a red dot) and six outer methylene hydrogen atoms (denoted as a blue dot), respectively, indicating that a square-pyramidal 1:1 complex between **1** and DABCO is formed with 0.5 equiv of free **1** (Figure 9a). The upfield shift and the chemical shift difference between the inner and outer hydrogen atoms

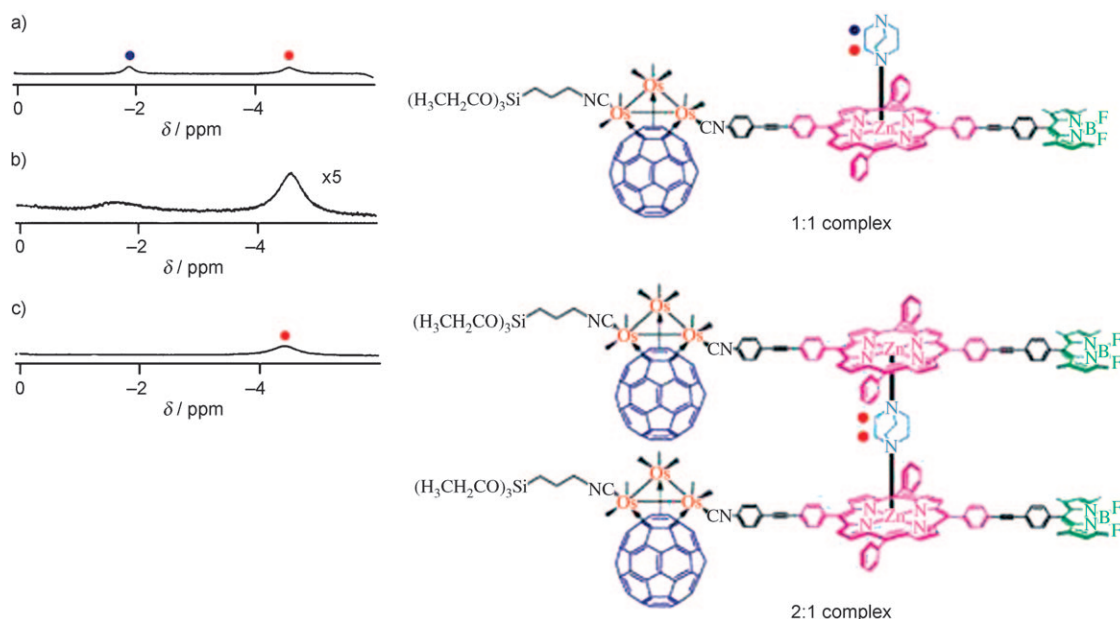
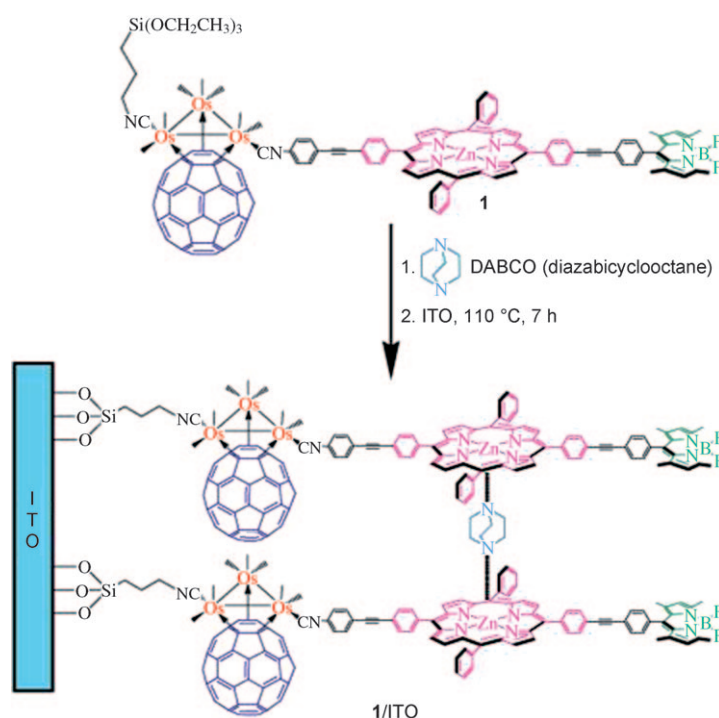


Figure 9. DABCO hydrogen resonances of **1**-DABCO complexes in a) 5.5 mM, b) 8.8 mM, and c) 17 mM **1** in CDCl_3 .

were attributed to the well-known ring-current effect of the porphyrin ring. At a higher concentration (17 mM) of **1**, however, a single resonance at -1.88 ppm was observed for the 12 methylene hydrogen atoms of DABCO, which implies formation of a 2:1 complex between **1** and DABCO (Figure 9c). At the intermediate concentration of 8.8 mM, the increase in the intensity ratio of the two resonances at -4.61 and -1.88 ppm is indicative of a higher concentration of the 2:1 complex than the 1:1 complex, as expected (Figure 9b). Upon formation of the 1:1 or 2:1 complex, the resonance of the β -hydrogen atoms of the pyrrole ring in ZnP shifts upfield by 0.15–0.35 ppm, reflecting the electron-donor effect of the DABCO ligand. Similar concentration-dependent complexations and the upfield shift of ZnP hydrogen atoms have been reported previously in the interaction of zinc-porphyrin derivatives and DABCO forming the 1:1 or 2:1 complex.^[23]

Formation of 1/ITO SAM: The SAM of **1** (**1**/ITO) has been prepared by immersion of an ITO electrode in a CB solution of **1** and DABCO (2:1 equiv) at 100°C for 7 h, followed by washing with CB and dichloromethane (DCM; Scheme 3). The absorption spectrum of **1**/ITO (Figure 10) shows a characteristic Soret band at $\lambda_{\text{max}} = 434$ nm, which is broader and red-shifted by approximately 7 nm relative to that of **1** in solution. The broadening and bathochromic shift indicate moderate perturbation within SAMs, mainly due to DABCO binding and porphyrin aggregation.

The water contact angle ($\theta_{\text{H}_2\text{O}}$) of 70° for **1**/ITO is increased substantially from $\theta_{\text{H}_2\text{O}} = 45^\circ$ for bare ITO (Figure S6 in the Supporting Information), which is consistent with adsorption of hydrophobic **1** on the ITO surface. The X-ray photoelectron spectra (XPS) further confirm the formation of **1**/ITO by detection of C(1s), N(1s), O(1s), F(1s),



Scheme 3. Formation of **1**/ITO SAM.

Si(2p), Zn(2p), and Os(4f) peaks involved in the SAM, as shown in Figure S7 in the Supporting Information.

The CVs of **1**/ITO in the ZnP oxidation region, with and without DABCO, reveal two well-resolved one-electron redox waves at $E_{1/2} = 0.41$, and 0.69 V for the ZnP oxidations (Figure 11); in the CV of **1**/ITO there is also a reversible one-electron redox wave at $E_{1/2} = -1.20$ V for the first reduction of the C_{60} cage (Figure 11, inset). Other redox cou-

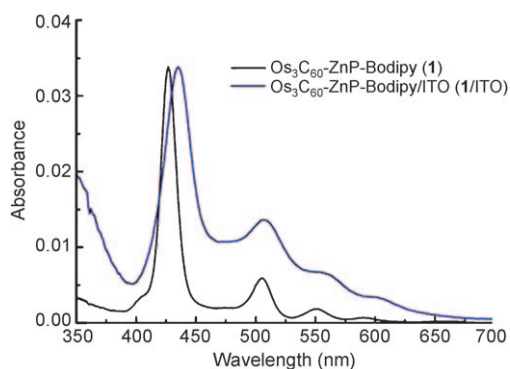


Figure 10. UV/Vis absorption spectra of **1** and **1/ITO** in CB.

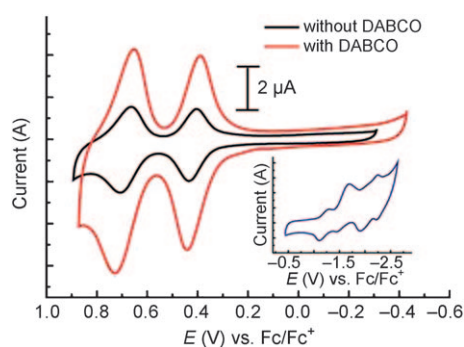


Figure 11. Cyclic voltammogram of the ZnP oxidation region of **1/ITO** in DCM with 0.1 M Bu₄NPF₆ as electrolyte (scan rate 0.1 V s⁻¹). Inset: the reduction region of **1/ITO**.

ples, however, are broad and are not as well resolved as those of **1** in solution. Presumably this is because of the heterogeneous environment of electrochemically active species in the SAM. The monolayer surface coverage (Γ) of **1/ITO** with and without DABCO is estimated to be 1.2×10^{-10} and 0.5×10^{-10} mol cm⁻², respectively, from the integrated charge of the first oxidation peak at 0.41 V. This result indicates more than 85% surface coverage of **1/ITO**, based on the theoretical value of 1.4×10^{-10} mol cm⁻² calculated for a close-packed monolayer of **1** in perpendicular orientation to the ITO surface. Well-ordered structural confinement, through strong interaction of ZnP with a bifunctional base DABCO, may be responsible for this high surface coverage, as shown in Scheme 3. The red shift of the Soret band in the UV/Vis spectrum of **1** (see above) implies that the axial DABCO binding to the d_{z²} orbital of zinc lowers the energy of the porphyrin excited singlet state and also enhances the surface coverage of **1** on the ITO electrode.

Photoelectrochemical properties: Photocurrent measurements for **1/ITO** were carried out in 0.1 M Na₂SO₄ solution containing ascorbic acid (AsA; 50 mM) as a sacrificial electron donor, by using the three-electrode system of the modified ITO substrate as a working electrode, a Pt counter electrode, and a Ag/AgCl (3 M NaCl) reference electrode (denoted as a **1/ITO/AsA/Pt** cell). A stable anodic photocurrent

appeared immediately upon irradiation of the ITO electrode with $\lambda = 440$ nm light (0.546 mW cm^{-2}) at an applied potential of 0.1 V versus Ag/AgCl (3 M NaCl) and the response was repeated reversibly (Figure 12). The anodic photocur-

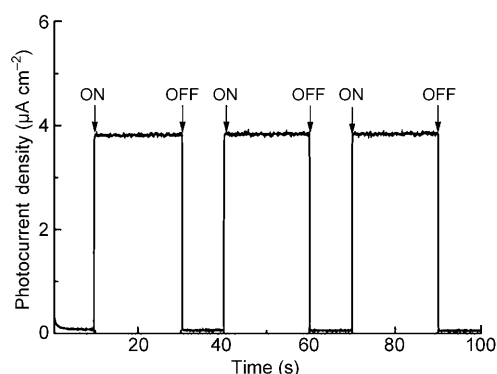


Figure 12. Photocurrent response of **1/ITO** irradiated with 440 nm light (0.546 mW cm^{-2}) and at an applied potential of 0.1 V vs. Ag/AgCl (3 M NaCl).

rent increased in proportion to an increase in the positive bias of the ITO electrode (Figure S8 in the Supporting Information). The action spectrum of the **1/ITO/AsA/Pt** cell, which is compared to the UV/Vis absorption spectra of **1/ITO** and **1** in CB in Figure 13, reveals a maximum current at 440 nm, indicating that porphyrin is a dominant photoactive sensitizer for photocurrent generation in this triad photoelectrochemical cell.

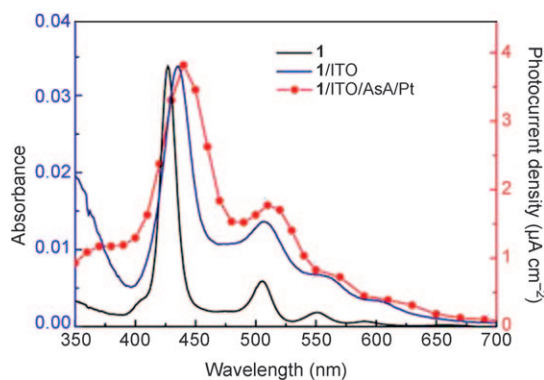


Figure 13. Absorption spectra of **1** and **1/ITO** and the action spectrum of a **1/ITO/AsA/Pt** cell irradiated with 0.546 mW cm^{-2} light at 0.1 V bias vs. Ag/AgCl.

The estimated quantum yield for the **1/ITO/AsA/Pt** cell is 29%, based on the number of photons absorbed by the chromophores, and its incident photon-to-current efficiency (IPCE) at 440 nm is 2.0%. The present triad **1/ITO/AsA/Pt** photoelectrochemical cell exhibits a remarkably high quantum yield, which is much higher than that of our previously reported dyad cell (19.5%) based on the Os₃C₆₀/ZnP array. This superior performance of the **1/ITO/AsA/Pt** photoelectrochemical cell might be attributed to the higher conjuga-

tion of the present triad **1** than of the previous dyad. In particular, the I/ITO/AsA/Pt cell has a much better light-harvesting property than the previously reported Os₃C₆₀-ZnP array, with absorption between 500–550 nm (Figure S9 in the Supporting Information) indicating efficient energy transfer from Bodipy to ZnP and electron transfer from ZnP to C₆₀ in the I/ITO/AsA/Pt cell. This triad photochemical cell has great potential for solving the poor light-harvesting properties of porphyrin^[24] molecules in the blue-green (450–600 nm) solar spectral regions and for mimicking natural photosynthetic systems through sequential energy and electron transfer.

Conclusion

We have successfully constructed a highly ordered, nearly fully covered [60]fullerene–triosmium cluster/zinc-porphyrin/boron–dipyrrin triad SAM on an ITO surface with the aid of DABCO. This cell exhibits the highest photocurrent generation efficiency, at 29%, ever reported for triad photoelectrochemical cells based on SAMs. The detailed kinetics involved in energy and electron transfer of the triad cluster have been fully elucidated by fluorescence-lifetime measurements and TA spectroscopic data. The remarkable quantum yield of our triad photoelectrochemical cell is attributed to the unique molecular characteristics of the cluster arrays: 1) they are thermally and electrochemically very stable, 2) they undergo facile electronic communication between C₆₀ and the metal cluster moieties, 3) the C₆₀–metal interaction in the μ₃-η²:η²:η²-C₆₀ bonding mode hardly perturbs the C₆₀ hybridization, 4) well-ordered structural confinement on the surface through strong interaction between the Zn²⁺ ion and the bifunctional DABCO base results in an extremely high surface coverage of the SAM, and 5) efficient energy transfer from Bodipy to ZnP and electron transfer from ZnP to C₆₀ occur due to the excellent light-harvesting property of Bodipy in the blue-green region. The present successful application of C₆₀–metal cluster complexes in photoelectrochemical cells promises other useful technological applications of C₆₀–metal-cluster-based SAMs for molecular electronic device fabrication.

Experimental Section

General: All reactions were carried out under a nitrogen atmosphere by using standard Schlenk techniques. Solvents were dried over appropriate drying agents and distilled immediately before use. C₆₀ (99.5%, Southern Chemical Group LLC) was used without further purification. Anhydrous trimethylamine N-oxide (m.p. 255–230 °C) was obtained from Me₃NO·2H₂O (98%, Aldrich) by sublimation (three times) at 90–100 °C under vacuum. Silica gel (Fuji Silysia BW-200T) was used for flash column chromatography. 4-Ethynylbenzaldehyde,^[25] 4,4-difluoro-8-(4'-iodophenyl)-1,3,5,7-tetramethyl-4-bora-3a,4a-diaza-s-indacene,^[26] meso-phenyldipyrrromethane,^[27] N-(4-ethynylphenyl)formamide,^[28] Os₃(CO)₈(CN(CH₂)₂Si(OEt)₃)(μ₃-η²:η²:η²-C₆₀) (**6**),^[29] and Os₃(CO)₇-(CNCH₂Ph)₂(μ₃-η²:η²:η²-C₆₀) (**8**)^[16] were prepared according to published methods. Infrared spectra were obtained with a Bruker Equinox-55 FTIR

spectrophotometer. ¹H (400 MHz), ¹¹B (96 MHz), and ¹⁹F (282 MHz) NMR spectra were recorded on Bruker Avance-400, AM 300, and DRX 300 spectrometers, respectively. Chemical shifts of ¹H, ¹¹B, and ¹⁹F NMR spectra were referenced to tetramethylsilane, boron trifluoride etherate, and chlorofluoromethane, respectively. MALDI-TOF mass spectra were obtained on a Voyager DE-STR spectrometer. Elemental analyses were performed on a Fisons EA1110 elemental analyzer. The syntheses of **1**, **2**, **3**, **4**, and **5** are described in the Supporting Information.

Preparation of I/ITO: An ITO glass was cleaned with acetone and dried by blowing a N₂ stream over the surface. The ITO electrode was immersed in a CB solution containing **1** and DABCO (total concentration 1 mM; molar ratio **1**/DABCO=2:1) at 100 °C for 7 h under an argon atmosphere. The electrode was rinsed and sonicated in CB to remove physisorbed **1**, then washed three times with CB and DCM.

Electrochemical measurements: Cyclic voltammetry was carried out on an Autolab PGSTAT 10 electrochemical analyzer (Eco Chemie, The Netherlands) using the conventional three-electrode system of a platinum working electrode (1.6 mm diameter disk, Bioanalytical Systems), a platinum-wire counter electrode (wire length 5 cm, diameter 0.5 mm), and a Ag/Ag⁺ reference electrode (0.1 M AgNO₃/Ag in acetonitrile with a VycorTM salt bridge). All measurements were performed at ambient temperature under a nitrogen atmosphere in a deoxygenated [(*n*Bu)₄N]ClO₄ (0.1 M) solution in dry CB. The analyte concentration was approximately 3 × 10⁻⁴ M. All potentials were referenced to the ferrocene/ferrocenium (Fc/Fc⁺) standard. The relative number of electrons involved in each reduction process was obtained from a graph of current versus time^{-1/2} according to the Cottrell equation.^[30]

Electrochemical measurement of I/ITO: Cyclic voltammetry was carried out with an AUTOLAB PGSTAT 10 electrochemical analyzer, using the conventional three-electrode system of a modified ITO working electrode (electrode area 0.39 cm²), a platinum-wire counter electrode (wire length 5 cm, diameter 0.5 mm), and a Ag QRE reference electrode. All measurements were performed at ambient temperature under a nitrogen atmosphere in a [(*n*Bu)₄N]PF₆ solution (0.1 M) in dry DCM. All potentials were referenced to the Fc/Fc⁺ standard. Surface coverage (Γ mol cm⁻²) was calculated from Γ = Q/nF. The charge density Q (μC cm⁻²) was calculated by integrating the faradaic current peak after subtracting a baseline of the charging current at a unit area of electrode. F is the Faraday constant and n is the number of electrons transferred. The real surface area of the ITO electrode (0.39 cm²) was determined by the electrochemical method based on mass-transfer and adsorption processes.

Photoelectrochemical measurements: Photoelectrochemical measurements were performed on I/ITO in a specially designed Teflon cell illuminated with monochromatic excitation light through a monochromator (Thermo Oriel, model 77250) by a 300 W xenon lamp (Thermo Oriel, model 6259). The photocurrent was measured in a three-electrode arrangement (Gamry, Reference 600), a modified ITO working electrode, a platinum-wire counter electrode, and a Ag/AgCl (3 M NaCl) reference electrode. The light intensity was monitored by an optical power meter (Newport 1830-C) and corrected. The quantum yield and IPCE of the photocurrent generation were obtained from φ = (i/e)/[I(1-10⁻⁴)] and IPCE (%) = 100 × 1240 × I_{sc}/(Wλ), in which I = (Wλ)/(hc), i is the photocurrent density, e is the elementary charge, I is the number of photons per unit area and unit time, λ is the wavelength of light irradiation, A is the absorbance of adsorbed dyes at λ nm, W is the light power irradiated at λ nm, c is the velocity of light, h is the Planck constant, and I_{sc} is the short-circuit photocurrent.

Time-resolved fluorescence measurements: Each of the samples was dissolved in CB (Aldrich, Spectroscopic Grade). Sample concentrations were approximately 0.5 mM. In time-resolved experiments, a cuvette (200 μm thick) containing the sample solution was mounted on a homemade shaking stage, with a speaker to minimize photodamage. All the experiments were carried out at ambient temperature. Picosecond TRF was measured by the time-correlated single-photon counting (TCSPC) method. Light sources were a homebuilt, cavity-dumped optical parametric oscillator (OPO)^[31] and a homebuilt optical parametric amplifier (OPA), which provided visible pulses at 550 and 500 nm, respectively. In TCSPC, a singlet lens was used to focus the excitation beam onto the

sample and the fluorescence was collected in a back-scattering geometry by using a parabolic mirror. The emission was sent to a monochromator and detected with a thermoelectrically cooled MCP-PMT (Hamamatsu R3809U-51). Magic-angle detection was used to avoid the effect of polarization. The full width at half maximum (FWHM) of the instrumental response was 40 ps, to provide time resolution better than 10 ps after deconvolution. Femtosecond time resolution in TRF was achieved by fluorescence up-conversion. The apparatus with time resolution of 50 fs has been described in detail previously.^[32]

Transient absorption measurements: All the samples were prepared and handled similarly to those described for the TRF measurements. Light sources were based on a homebuilt multipass Ti:sapphire amplifier and an OPA system operating at 10 kHz. The OPA outputs of wavelengths 500 and 550 nm were used as pump pulses. For the single-color probe TA experiment, a white-light continuum was generated by self-phase modulation in a sapphire window 1 mm thick. Probe beams at 650 and 1000 nm were obtained from the white-light continuum by using interference band-pass filters, and these were focused directly into the sample without pulse compression. Time resolution from the cross-correlation measurement was about 200 fs. In the case of TA spectra measurement, white light continuum pulses in the visible and NIR regions were generated by self-phase modulation in a sapphire window 1 mm thick and a photonic crystal fiber, respectively. The continuum pulses were divided into two portions, the probe and reference beams, and sent to a monochromator (SP300i, Acton) through a bifurcated optical fiber, to be detected simultaneously by a CCD (charge-coupled device) detector (DV-420-0E, Andor).

Computational details: The calculations were based on DFT at the generalized gradient approximation (GGA) level (Becke's 1988 functional for exchange and Perdew-Wang's 1991 functional for correlation, BPW91^[33]). The energy-consistent relativistic effective core potential (RECP) was used for Zn and Os atoms.^[34] Double numerical plus polarization (DNP) basis sets were used for the C, H, B, N, O, and F atoms, and the valence electrons for Zn and Os were also expanded by using the DNP basis set. All the structures were optimized without any symmetry restriction by using the analytical gradients of the energies. The DMol3 program of the software package Material Studio from Accelrys^[35] was used for the geometry optimization and the MO analysis.

Acknowledgements

This work was supported by the Korea Research Foundation (Grant no. KRF-2005-201-C00021), the Korean Government (MOEHRD), the Korea Science and Engineering Foundation (KOSEF) Nano R&D program (Grant no. 2005-02618), the Korean Ministry of Science & Technology (MOST), and by the National Research Foundation of Korea Grant (20100001484), the Korean Government. T.J. acknowledges the support from KOSEF grant funded by the Korea Government (MEST; Grant no. R11-2008-012-01001-0).

- [1] a) M. R. Wasielewski, *Chem. Rev.* **1992**, *92*, 435–461; b) D. Gust, T. A. Moore, A. L. Moore, *Acc. Chem. Res.* **2001**, *34*, 40–48.
 [2] a) T. Akiyama, H. Imahori, A. Ajavakom, Y. Sakata, *Chem. Lett.* **1996**, 907–908; b) H. Yamada, H. Imahori, Y. Nishimura, I. Yamazaki, T. K. Ahn, S. K. Kim, D. Kim, S. Fukuzumi, *J. Am. Chem. Soc.* **2003**, *125*, 9129–9139; c) H. Imahori, H. Yamada, Y. Nishimura, I. Yamazaki, Y. Sakata, *J. Phys. Chem. B* **2000**, *104*, 2099–2108; d) H. Imahori, M. Kimura, K. Hosomizu, T. Sato, T. K. Ahn, S. K. Kim, D. Kim, Y. Nishimura, Y. Iwao, Y. Araki, O. Ito, S. Fukuzumi, *Chem. Eur. J.* **2004**, *10*, 5111–5122; e) H. Imahori, H. Norieda, H. Yamada, Y. Nishimura, I. Yamazaki, Y. Sakata, S. Fukuzumi, *J. Am. Chem. Soc.* **2001**, *123*, 100–110; f) A. Ikeda, T. Hatano, S. Shinkai, T. Akiyama, S. Yamada, *J. Am. Chem. Soc.* **2001**, *123*, 4855–4856; g) V. Chukharev, T. Vuorinen, A. Efimov, N. V. Tkachenko, M. Kimura, S. Fukuzumi, H. Imahori, H. Lemmetyinen, *Langmuir*

- 2005**, *21*, 6385–6391; h) S. Kang, T. Umeyama, M. Ueda, Y. Matano, H. Hotta, K. Yoshida, S. Isoda, M. Shiro, H. Imahori, *Adv. Mater.* **2006**, *18*, 2549–2552; i) T. Hasobe, H. Imahori, P. V. Kamat, T. K. Ahn, S. K. Kim, D. Kim, A. Fujimoto, T. Hirakawa, S. Fukuzumi, *J. Am. Chem. Soc.* **2005**, *127*, 1216–1228; j) Y. Matsuo, K. Kanaizuka, K. Matsuo, Y. Zhong, T. Nakae, E. Nakamura, *J. Am. Chem. Soc.* **2008**, *130*, 5016–5017.
 [3] a) H. Imahori, S. Fukuzumi, *Adv. Funct. Mater.* **2004**, *14*, 525–536; b) D. Bonifazi, O. Enger, F. Diederich, *Chem. Soc. Rev.* **2007**, *36*, 390–414.
 [4] a) D. M. Guldi, C. Luo, M. Prato, A. Troisi, F. Zerbetto, M. Scheffoske, E. Dietel, W. Bauer, A. Hirsh, *J. Am. Chem. Soc.* **2001**, *123*, 9166–9167; b) T. D. M. Bell, T. A. Smith, K. P. Ghiggino, M. G. Ranasinghe, M. J. Shephard, M. N. Paddon-Row, *Chem. Phys. Lett.* **1997**, *268*, 223–228; c) H. Imahori, K. Hagiwara, T. Akiyama, M. Aoki, S. Taniguchi, T. Okada, M. Shirakawa, Y. Sakata, *Chem. Phys. Lett.* **1996**, *263*, 545–550; d) H. Imahori, H. Yamada, D. M. Guldi, Y. Endo, A. Shimomura, S. Kundu, K. Yamada, T. Okada, Y. Sakata, S. Fukuzumi, *Angew. Chem.* **2002**, *114*, 2450–2453; *Angew. Chem. Int. Ed.* **2002**, *41*, 2344–2347; e) A. Lembo, P. Tagliatesta, D. M. Guldi, *J. Phys. Chem. A* **2006**, *110*, 11424–11434; f) L. Sanchez, M. Sierra, N. Martín, A. J. Myles, T. J. Dale, J. Rebek, Jr., W. Seitz, D. M. Guldi, *Angew. Chem.* **2006**, *118*, 4753–4757; *Angew. Chem. Int. Ed.* **2006**, *45*, 4637–4641; g) F. D'Souza, G. R. Deviprasad, M. E. Zandler, V. T. Hoang, K. Arkady, M. VanStipdonk, A. Perera, M. E. El-Khouly, M. Fujitsuka, O. Ito, *J. Phys. Chem. A* **2002**, *106*, 3243–3252; h) D. I. Schuster, K. Li, D. M. Guldi, A. Palkar, C. S. Echegoyen, R. J. Cross, M. Niemi, N. V. Tkachenko, H. Lemmetyinen, *J. Am. Chem. Soc.* **2007**, *129*, 15973–15982.
 [5] a) D. M. Guldi, M. Maggini, G. Scorrano, M. Prato, *J. Am. Chem. Soc.* **1997**, *119*, 974–980; b) M. Fujitsuka, N. Tsuboya, R. Hamasaki, M. Ito, S. Onodera, O. Ito, Y. Yamamoto, *J. Phys. Chem. A* **2003**, *107*, 1452–1458; c) G. A. Rajkumar, A. S. D. Sandanayaka, K. Ikeshta, Y. Araki, Y. Furusho, T. Takata, O. Ito, *J. Phys. Chem. B* **2006**, *110*, 6516–6525; d) F. Caporossi, B. Floris, P. Galloni, E. Gatto, M. Venanzi, *Eur. J. Org. Chem.* **2006**, 4362–4366.
 [6] K. Matsumoto, M. Fujitsuka, T. Sato, S. Onodera, O. Ito, *J. Phys. Chem. B* **2000**, *104*, 11632–11638.
 [7] F. D'Souza, R. Chitta, A. S. D. Sandanayaka, N. K. Subbaiyan, L. D'Souza, Y. Araki, O. Ito, *J. Am. Chem. Soc.* **2007**, *129*, 15865–15871.
 [8] a) C. Luo, D. M. Guldi, H. Imahori, K. Tamaki, Y. Sakata, *J. Am. Chem. Soc.* **2000**, *122*, 6535–6536; b) H. Imahori, K. Tamaki, D. M. Guldi, C. Luo, M. Fujitsuka, O. Ito, Y. Sakata, S. Fukuzumi, *J. Am. Chem. Soc.* **2001**, *123*, 2607–2617; c) H. Imahori, D. M. Guldi, K. Tamaki, Y. Yoshida, C. Luo, Y. Sakata, S. Fukuzumi, *J. Am. Chem. Soc.* **2001**, *123*, 6617–6628; d) H. Imahori, Y. Sekiguchi, Y. Kashiwagi, T. Sato, Y. Araki, O. Ito, H. Yamada, S. Fukuzumi, *Chem. Eur. J.* **2004**, *10*, 3184–3196; e) D. Kuciauskas, P. A. Liddell, S. Lin, T. E. Johnson, S. J. Weghorn, J. S. Lindsey, A. L. Moore, T. A. Moore, D. Gust, *J. Am. Chem. Soc.* **1999**, *121*, 8604–8614; f) F. D'Souza, O. Ito, *Coord. Chem. Rev.* **2005**, *249*, 1410–1422.
 [9] a) D. M. Guldi, *Chem. Soc. Rev.* **2002**, *31*, 22–36; b) D. M. Guldi, *Phys. Chem. Chem. Phys.* **2007**, *9*, 1400–1420.
 [10] F. D'Souza, P. M. Smith, M. E. Zandler, A. L. McCarty, M. Itou, Y. Araki, O. Ito, *J. Am. Chem. Soc.* **2004**, *126*, 7898–7907.
 [11] a) A. Ulman, *An Introduction to Ultrathin Organic Films: From Langmuir-Blodgett to Self-Assembly*, Academic Press, San Diego, **1991**; b) A. Ulman, *Chem. Rev.* **1996**, *96*, 1533–1554; c) C. A. Mirkin, *Inorg. Chem.* **2000**, *39*, 2258–2272; d) A. N. Shipway, E. Katz, I. Willner, *ChemPhysChem* **2000**, *1*, 18–52; e) A. P. Alivisatos, P. F. Barbara, A. W. Castleman, J. Chang, D. A. Dixon, M. L. Klein, G. L. McLendon, J. S. Miller, M. A. Ratner, P. J. Rossky, S. I. Stupp, M. E. Thompson, *Adv. Mater.* **1998**, *10*, 1297–1336; f) S. Flink, F. C. J. M. Veggel, D. N. Reinhoudt, *Adv. Mater.* **2000**, *12*, 1315–1328; g) T. P. Sullivan, W. T. S. Huck, *Eur. J. Org. Chem.* **2003**, 17–29.

- [12] Y.-J. Cho, T. K. Ahn, H. Song, K. S. Kim, C. Y. Lee, W. S. Seo, K. Lee, S. K. Kim, D. Kim, J. T. Park, *J. Am. Chem. Soc.* **2005**, *127*, 2380–2381.
- [13] a) R. P. Haugland in *The Handbook A Guide to Fluorescent Probes and Labeling Technologies*, 10th ed. (Ed.: M. T. Z. Spence), Molecular Probes, Eugene, **2005**; b) H. C. Kang, R. P. Haugland, U.S. Patent 5451663, **1995**; c) A. Burghart, H. Kim, M. B. Welch, L. H. Thoresen, J. Reibenspies, K. Burgess, *J. Org. Chem.* **1999**, *64*, 7813–7819; d) J. Chen, A. Burghart, A. Derecskei-Kovacs, K. Burgess, *J. Org. Chem.* **2000**, *65*, 2900–2906; e) B. Turfan, E. U. Akkaya, *Org. Lett.* **2002**, *4*, 2857–2859; f) A. Coskun, E. U. Akkaya, *J. Am. Chem. Soc.* **2005**, *127*, 10464–10465; g) W. Qin, T. Rohand, M. Baruah, A. Stefan, M. Van der Auweraer, W. Dehaen, N. Boens, *Chem. Phys. Lett.* **2006**, *420*, 562–568.
- [14] H. Martin, H. Rudolf, F. Vlastimil, *Fluorescence Spectroscopy in Biology: Advanced Methods and their Applications to Membranes, Proteins, DNA, and Cells*, Springer, Heidelberg, **2005**.
- [15] a) R. W. Wagner, J. S. Lindsey, *J. Am. Chem. Soc.* **1994**, *116*, 9759–9760; b) R. W. Wagner, J. S. Lindsey, J. Seth, V. Palaniappan, D. F. Bocian, *J. Am. Chem. Soc.* **1996**, *118*, 3996–3997.
- [16] C. Y. Lee, B. K. Park, J. H. Yoon, C. S. Hong, J. T. Park, *Organometallics* **2006**, *25*, 4634.
- [17] H. Song, K. Lee, J. T. Park, M. G. Choi, *Organometallics* **1998**, *17*, 4477–4483.
- [18] a) A. Z. Weller, *Phys. Chem.* **1982**, *132*, 93; b) D. Rehm, A. Weller, *Isr. J. Chem.* **1970**, *10*, 529.
- [19] J. Rodriguez, C. Kirmaier, D. Holten, *J. Am. Chem. Soc.* **1989**, *111*, 6500–6506.
- [20] D. Kim, M. Lee, Y. D. Suh, S. K. Kim, *J. Am. Chem. Soc.* **1992**, *114*, 4429–4430.
- [21] J. I. Steinfeld, J. S. Francisco, W. L. Hase, *Chemical Kinetics and Dynamics*, 2nd ed., Prentice Hall, Portage, **1999**.
- [22] T. Elsaesser, W. Kaiser, *Annu. Rev. Phys. Chem.* **1991**, *42*, 83–107.
- [23] a) C. A. Hunter, M. N. Meah, J. K. M. Sanders, *J. Am. Chem. Soc.* **1990**, *112*, 5773–5780; b) D. M. Guldi, C. Luo, T. D. Ros, M. Prato, E. Diotel, A. Hirsh, *Chem. Commun.* **2000**, 375–376.
- [24] H. Imahori, T. Umeyama, S. Ito, *Acc. Chem. Res.* **2009**, *42*, 1809–1818.
- [25] T. Sasaki, J.-F. Morin, M. Lu, J. M. Tour, *Tetrahedron Lett.* **2007**, *48*, 5817–5820.
- [26] T. A. Golovkova, D. V. Kozlov, D. C. Neckers, *J. Org. Chem.* **2005**, *70*, 5545.
- [27] C.-H. Lee, J. S. Lindsey, *Tetrahedron* **1994**, *50*, 11427–11440.
- [28] J. M. Tour, A. M. Rawlett, M. Kozaki, Y. X. Yao, R. C. Jagessar, S. M. Dirk, D. W. Price, M. A. Reed, C. W. Zhou, J. Chen, W. Y. Wang, I. Campbell, *Chem. Eur. J.* **2001**, *7*, 5118–5134.
- [29] Y.-J. Cho, H. Song, K. Lee, K. Kim, J. Kwak, S. Kim, J. T. Park, *Chem. Commun.* **2002**, 2966–2967.
- [30] A. J. Bard, L. R. Faulkner in *Electrochemical Methods*, Wiley, New York, **1980**, pp. 142–146.
- [31] C.-K. Min, T. Joo, *Opt. Lett.* **2005**, *30*, 1855–1857.
- [32] H. Rhee, T. Joo, *Opt. Lett.* **2005**, *30*, 96–98.
- [33] a) A. D. Becke, *Phys. Rev. A* **1988**, *38*, 3098–3100; b) J. P. Perdew, Y. Wang, *Phys. Rev. B* **1992**, *45*, 13244–13249.
- [34] D. Andrae, U. Häußermann, M. Dolg, H. Stoll, H. Preuß, *Theor. Chim. Acta* **1990**, *77*, 123–141.
- [35] a) B. Delley, *J. Chem. Phys.* **1990**, *92*, 508–517; b) B. Delley, *J. Chem. Phys.* **2000**, *113*, 7756–7764.

Received: January 26, 2010

Published online: April 16, 2010